ARTICLE IN PRESS

FEBS Letters xxx (2013) xxx–xxx

FEBS Letters

journal homepage: www.FEBSLetters.org

Effect of the amyloid β hairpin's structure on the handedness of helices formed by its aggregates ☆

Pavan K. GhattyVenkataKrishna [a,b,*], Edward C. Uberbacher [a,b], Xiaolin Cheng [b,c,d]

[a] Computational Biology and Bioinformatics Group, Oak Ridge National Laboratory, Oak Ridge, TN, USA
[b] BioEnergy Science Center, Oak Ridge National Laboratory, Oak Ridge, TN, USA
[c] Department of Biochemistry and Cellular and Molecular Biology, University of Tennessee, Knoxville, TN, USA
[d] UT/ORNL Center for Molecular Biophysics, Oak Ridge National Laboratory, Oak Ridge, TN, USA

ARTICLE INFO

Article history:
Received 19 February 2013
Revised 16 May 2013
Accepted 21 June 2013
Available online xxxx

Edited by Robert B. Russell

Keywords:
Amyloid
Alzheimer's
Protein structure

ABSTRACT

Various structural models for amyloid β fibrils have been derived from a variety of experimental techniques. However, these models cannot differentiate between the relative position of the two arms of the β hairpin called the stagger. Amyloid fibrils of various hierarchical levels form left-handed helices composed of β sheets. However it is unclear if positive, negative and zero staggers all form the macroscopic left-handed helices. To address this issue we have conducted extensive molecular dynamics simulations of amyloid β sheets of various staggers and shown that only negative staggers lead to the experimentally observed left-handed helices while positive staggers generate the incorrect right-handed helices. This result suggests that the negative staggers are physiologically relevant structure of the amyloid β fibrils.

© 2013 The Authors. Published by Elsevier B.V. All rights reserved.

1. Introduction

Misfolding of peptide fragments into large fibrillar structures has been implicated in a variety of human diseases [1,2]. Alzheimer's related plaque formation is of particular interest due to its prevalence, high economic cost [3] and lack of effective treatment and/or preventive protocols. The fibrillar structure in Alzheimer's disease is formed due to misfolding of amyloid β (Aβ) peptide. Human Aβ42 peptides with the sequence, D_1AEFRHDSGY_{10} EVHHQKL$_{17}$VFF$_{20}$ AEDVGSNKGA$_{30}$ IIGLMVGGVV$_{40}$IA$_{42}$, are formed by the endoprotelytic cleavage of β-Amyloid-Precursor-Protein (APP) [4] by two proteases, β and γ secretase. Depending on the point of cleavage, peptides of length 40/42 are formed; usually in a ratio of 10:1 [5,6]). These peptides have ordered regions (9–26 and 31–42) [7–9] punctuated by a loop region (27–30) which makes the two ordered domains fall over one another forming a hairpin structure. Residues 1–8 were found to be disordered and not necessary for fibril formation [10]. Although the exact demarcation of the ordered and loop regions differs from one study to another, most agree that there is a hairpin structure which forms higher order aggregates and extends infinitely to form an fibril. In amyloid fibrils, the β sheets run perpendicular to the fiber axis and the inter-chain hydrogen bonds are roughly parallel to the fiber axis [11–14].

The inherent difficulty in obtaining crystals of full-length amyloid peptides has led a generation of researchers to employ a range of tools to characterize the structures. Solid-state NMR [15–26], Fourier Transform Infrared spectroscopy (FTIR) [27–29], circular dichroism (CD) [30], X-ray fiber diffraction [31–33], electron microscopy (EM) [12], hydrogen/deuterium exchange [21,34–41], proline-scanning mutagenesis [42,43], electron paramagnetic resonance (EPR) [44–46], and Raman spectroscopy [32,47] have been used to study both full length and fragments of the peptide. Although the studies generally agree with the cross-β sheet arrangement of the fibrils, there are disagreements in the exact organization of the β hairpin. For example, F19/L34 stacking was proposed by a Petkova et al. [7] while D22/L34 stacking was proposed by Lührs et al. [8]. At the next level of organization, models with a cross-section of two or three hairpins have been proposed. Within dimers, N-terminal/N-terminal, C-terminal/C-terminal (CC) and C-terminal/N-terminal stacking seem possible, although support for the CC stacking represented by C_{2z} structure is mounting [7,48]. Fig. 3 in Ref. [49] contains a comprehensive list of possible dimers. Nanopores formed by Aβ hairpin trimers have also been proposed [50–52].

In addition to many full-length amyloid peptides there is also a great body of work, both experimental and theoretical, on various fragments of the peptide many of which form amyloid-like β

☆ This is an open-access article distributed under the terms of the Creative Commons Attribution-NonCommercial-No Derivative Works License, which permits non-commercial use, distribution, and reproduction in any medium, provided the original author and source are credited.

* Corresponding author at: Computational Biology and Bioinformatics Group, Oak Ridge National Laboratory, Oak Ridge, TN 37831, USA.

E-mail addresses: pkc@ornl.gov, pavanghatty@gmail.com (P.K. GhattyVenkata Krishna).

0014-5793/$36.00 © 2013 The Authors. Published by Elsevier B.V. All rights reserved.
http://dx.doi.org/10.1016/j.febslet.2013.06.050

sheets. Computer simulation efforts include studies of Aβ fragments 16–22, 16–35, 10–35 [53], 22–27, 22–29 [54], 25–35 (and its N27Q mutant) [55], 25–35 [56], 17–42 (monomer and dimer) [57], and 9–40 [58,59]. Experimental efforts include the following Aβ fragments: 10–35 [60], 18–28, 16–28, 14–28, 12–28, 1–28, 20–28 [61,62], 11–25 [63,64], 16–22 [15,65], 10–23 [10], 14–23 [66,67], 25–35 [68], 37–42, 35–40 [69]. For a comprehensive list of Aβ fragment studies please refer to Table 2 in Serpell [30] and more recently Fig. 1 in Fändrich [9]. A recent study combined atomic force microscopy with molecular dynamics simulations to study the aggregation properties of the hydrophobic fragment 12–24 and found the β sheet structure to be highly pH dependent [70]. Differences among experimental studies can be attributed to the preparation protocol, solvent, pH and most importantly the techniques used to make observations. In a similar fashion, differences in the computer simulation studies can be attributed to preparation protocol, time scale, force field and, as we argue in this study, heavily to the choice of initial structures.

The presence of stagger where the C-terminal of chain i interacts with the N–terminal of chain $i \pm 1$ or $i \pm 2$ has been noted in literature [7,8]. Although solid state NMR data was used to determine the magnitude of the stagger (C-terminal of chain i is staggered by a distance of ±7.2 Åfrom N-terminal of the same chain), there is no clarity on the direction of the stagger. Due to the nature of contacts formed, positive and negative staggers of the same magnitude are structurally distinct [7]. Aβ amyloid fibrils of various hierarchical levels are always left-handed [71]. This raises an interesting question: Does the sign of the stagger have an effect on the twist of the helical turn in Aβ? To answer this question we conducted multiple simulations of a dimerized 20mer arranged in the C_{2z} [59] structure of Aβ(17–42), also known as p3 peptide [72–74], with no initial twist but with an initial stagger of 0, ±1, ±2, and ±3.

2. Methods and analysis

Full length amyloid peptides aggregate to form a hairpin structure with two layers of β sheets. Residues 17–24 comprise the top layer while 33–42 comprise the bottom layer. We refer to this as the fibril monomer. Although this monomer has been proposed to dimerize in various ways [59], the C_{2z} quaternary form is considered most stable [7,75,76]. We have therefore confined this study to C_{2z} conformation of the dimer. As shown in Fig. 1a, in a C_{2z} structure the C-terminals of the two monomers in a fibril cross-section interact in an anti-parallel fashion with symmetry along the z axis.

Two most cited structures of Aβ deposited in PDB are 2BEG (Aβ17–42) and 2LMN(O) (Aβ9–40). We used the 2BEG structure since the double mutants K28D/D23K and F19G/G38F and quadruple mutant F19A/A21F/V36G/G38F, all were shown to restore the ability to form wild type-like fibrils. This lends credence to the intra chain side–chain contacts described in 2BEG [8]. While the 2LMN(O) structure has its own strengths (more constraints than 2BEG and a structure of the dimer), the intra chain contacts described by 2BEG were deemed critical to the development of twist in the fibrils. Direct comparison of 2BEG and 2LMN(O) structures is difficult since it would require either keeping 2LMN(O) intact and adding residues 9–16 and deleting 41–42 in 2BEG or keeping 2BEG intact and deleting residues 9–16 and adding 41–42 in 2LMN(O). Either approach will result in one structure where one arm of the hairpin extends farther into the solvent than the other arm while the other structure has hairpin arms of roughly the same length.

Central chain of model 10 of 2BEG was used as the repeat unit. We define this chain as having a stagger of 1 since the C-terminal of chain i overlaps with the N-terminal of chain i 1. First a 20mer was generated by placing 20 chains along z-axis with a spacing of 4.8 Å[7,77,78] between each other. A 180° rotation around the z-axis resulted in another 20mer which completes the 40mer.

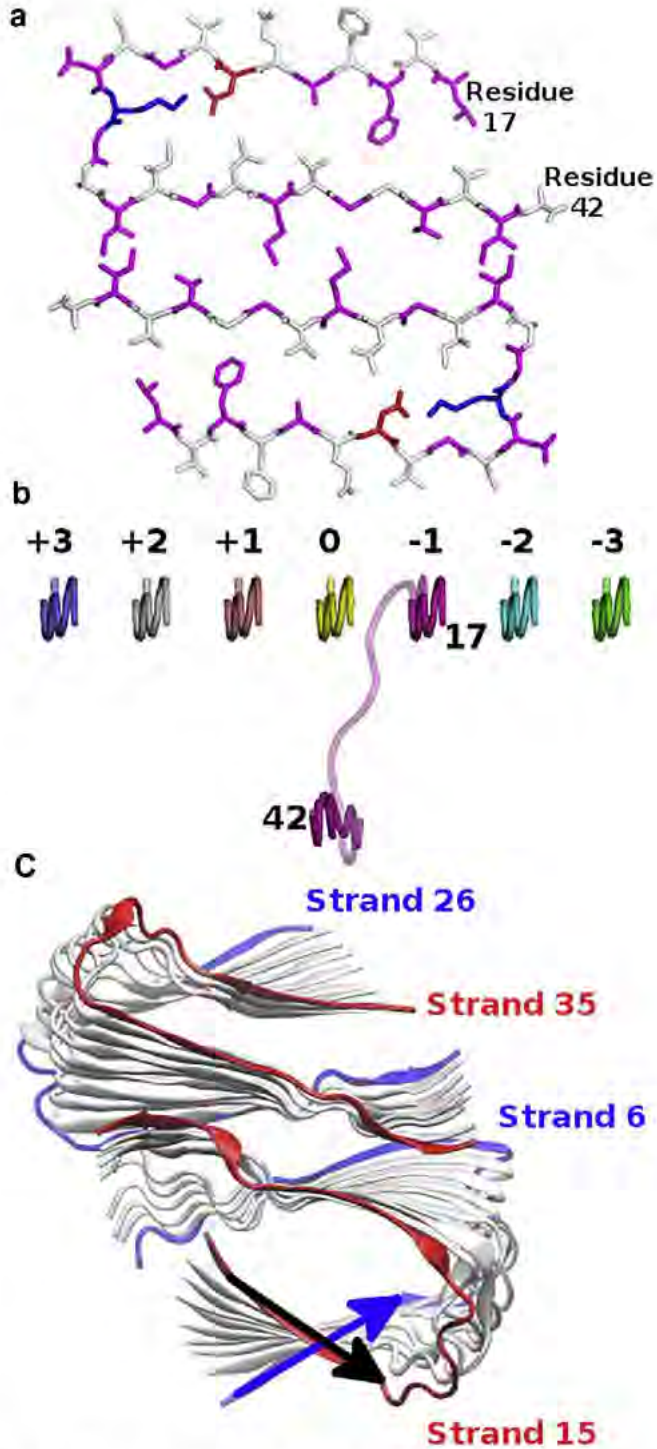

Fig. 1. (a) Schematic representation of the beginning structure. Residue D23 is in red, residue K28 is in blue, other even numbered residues are in white and odd numbered residues are in magenta. (b) Stagger −1 is in magenta and residues 17 and 42 are marked. In other staggers the position of residues 17–24 and the loop region changes with respect to residues 30–42. For the sake of clarity only residues 17–24 are show in other staggers. (c) Final structure of an Aβ sheet of stagger −3. Chains 6 and 26 are shown in blue while chains 15 and 35 are shown in red. Vector formed by joining Cα of residues 18 and 25 of chain 6 is shown as a blue arrow while a similar vector in chain 15 is shown as a black arrow. Average of the angles between these two vectors and between two similar vectors on chains 26 and 35 was used to determine the magnitude and sign of the twist. This figure shows a left handed helical turn of ~5° per chain.

The distance between the C-terminal β sheet plane of the 20mer on the top and that on the bottom was ensured to be 10 Å. The

Please cite this article in press as: GhattyVenkataKrishna, P.K., et al. Effect of the amyloid β hairpin's structure on the handedness of helices formed by its aggregates. FEBS Lett. (2013), http://dx.doi.org/10.1016/j.febslet.2013.06.050

Table 1
System sizes, number of runs, length of runs and initial twist of the seven staggers studied.

Stagger	Total atoms	Protein atoms	Sodium ions	Water atoms	Number of runs	Total simulation length (ns)	Initial twist (deg)
+3	70914	14960	40	55914	10	100	0
+2	68526	14960	40	53526	10	100	0
+1	66126	14960	40	51162	10	100	0
0	63852	14960	40	48852	10	100	0
−1	64641	14960	40	49641	10	100	0
−2	66954	14960	40	51954	10	100	0
−3	69270	14960	40	54270	10	100	0

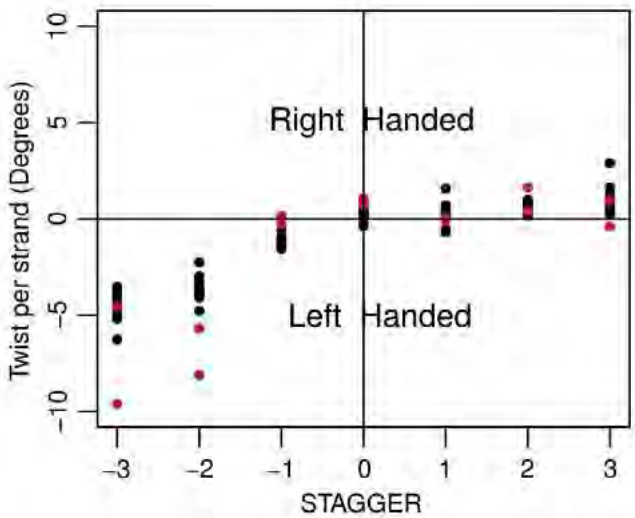

Fig. 2. Data from 10 separate runs starting with a stagger of 0, ±1, ±2, and ±3 and an intial twist of 0° (hairpin contacts are from 2BEG). Black dots correspond to data from 10 ns runs while red dots correspond to data from 90 ns runs. In the 10 ns studied, negative staggers result in left-handed helices while some positive staggers result in the unnatural right-handed helices. Error bars were not shown since the largest of the standard deviations from the 70 runs was only 0.4°. After 90 ns, all staggers except −2 and −3 revert back to neutral twist while stagger −2 and −3 retain significant twist per amyloid chain.

40mer created in this fashion has no twist and the M35 of the top and bottom 20mers pack to form a hydrophobic patch. The chains on the bottom fibril are numbered from 1–20 and the chains on the top fibril are numbered from 21–40 where chain 1 sits below chain 21 and chain 20 sits below chain 40.

After constructing stagger 1 as described above the N-terminal residues (17–24) were moved by 4.8 Åsuch that C-terminal of chain i now overlaps with N-terminal of chain i 2 resulting in stagger 2. Peptides thus made have an artificially elongated peptide bond between residues 24 and 25. This peptide bond of improper length was corrected by running a 20,000 step conjugate gradient energy minimization while keeping residues 17–24 and 34–42 fixed. This procedure was repeated as appropriate to obtain the other staggers 0, +1, +2, and ±3. Additional detail can be found in Fig. S1. Peptides with these staggers were then solvated in a water box with a padding distance of 15 Åfrom the protein. 40 sodium ions were added to neutralize each system. Table 1 lists the information for each system and Fig. 1a, b clarify the starting structures.

The solvated and charge-neutralized boxes were then minimized for 10,000 steps while keeping the backbone of the peptides fixed using a harmonic restraint of 5 kcal mol ^{1} Å ^{2}. After minimization, the temperature of the systems was set to 100 K and the harmonic restraints on the backbone were removed. The α carbon of residue M35 in chain 30, was fixed in all the simulations to arrest translation of the 40mer during the production run. After heating the systems from 100 K to 200 K in steps of 10 K/20 ps, 10 separate runs of each of the 7 staggers were conducted each with a different seed value to reinitialize velocities at 200 K. At this stage, all the 70 runs were heated from 200 K to 310 K again in steps of 10 K/20 ps. Upon reaching 310 K all the systems were equilibrated for one nanosecond (ns) after which 10 ns of data were collected and used for analysis. Further, 2 runs in each of the 7 staggers were randomly chosen and extended by 80 ns to a total of 90 ns. Thus a total of 1820 ns (7 × 10 × 10 + 7 × 2 × 80) of data were analyzed.

Table 2
Possible salt bridges in each stagger.

Stagger	D23 of chain i	Salt bridge with ...
−3	$D23_i$	$K28_{i\ 2}$, $K28_{i\ 3}$.
−2	$D23_i$	$K28_{i\ 1}$, $K28_{i\ 2}$.
−1	$D23_i$	$K28_i$, $K28_{i\ 1}$.
0	$D23_i$	$K28_i$, $K28_{i+1}$.
+1	$D23_i$	$K28_i$, $K28_{i+1}$.
+2	$D23_i$	$K28_{i+1}$, $K28_{i+2}$.
+3	$D23_i$	$K28_{i+2}$, $K28_{i+3}$.

NAMD 2.9 [79] with CHARMM27 force field [80](with CMAP corrections [81]) was used for performing these calculations. All the simulations were performed in the NPT ensemble. Langevin thermostat with a damping coefficient γ of 1 ps ^{1} was used for temperature control. Nosè–Hoover Langevin piston [82,83] with an oscillation period of 100 fs and damping time scale of 50 fs was used for pressure control. A time step of 2 fs was used during the entire length of the simulation. VMD [84] was used for data analysis, visualization and to generate pictures in both the main text and Supporting material.

The twist of the fibrils was calculated by considering only the central 20 chains, i.e. bottom chains 1–5, 16–20 and top chains 21–25 and 36–40 were ignored to eliminate any end-effects. As shown in Fig. 1c, the dot product of the vectors formed by joining CA_{18} and CA_{24} of chains 6 and 15 gives the magnitude of the twist angle for the bottom 10 central chains while the cross product of the vectors defines the direction of the twist. The twist angle was scaled down by a factor of 9 to obtain twist per chain. The same quantity was measured from chains 26 and 35 of the top fibril monomer and the average value of the top and bottom twist angle was reported.

3. Results

3.1. Twisting of fibers

Fig. 2 shows the mean values of twist as a function of the staggers. During the course of 10 ns simulations, the twist in each of the staggers develops from an initial value of 0 to the respective final value. Mean value from the last nanosecond of the 10 ns in each run is reported. The structure of the central 20 chains at the end of 10 ns in each of the 7 × 10 runs is shown in Fig. S2. It is clear from Fig. 2 that negative staggers lead to the experimentally observed left-handed helical turn while the positive staggers generate neutral or the unnatural right-handed helix. The extent of twist

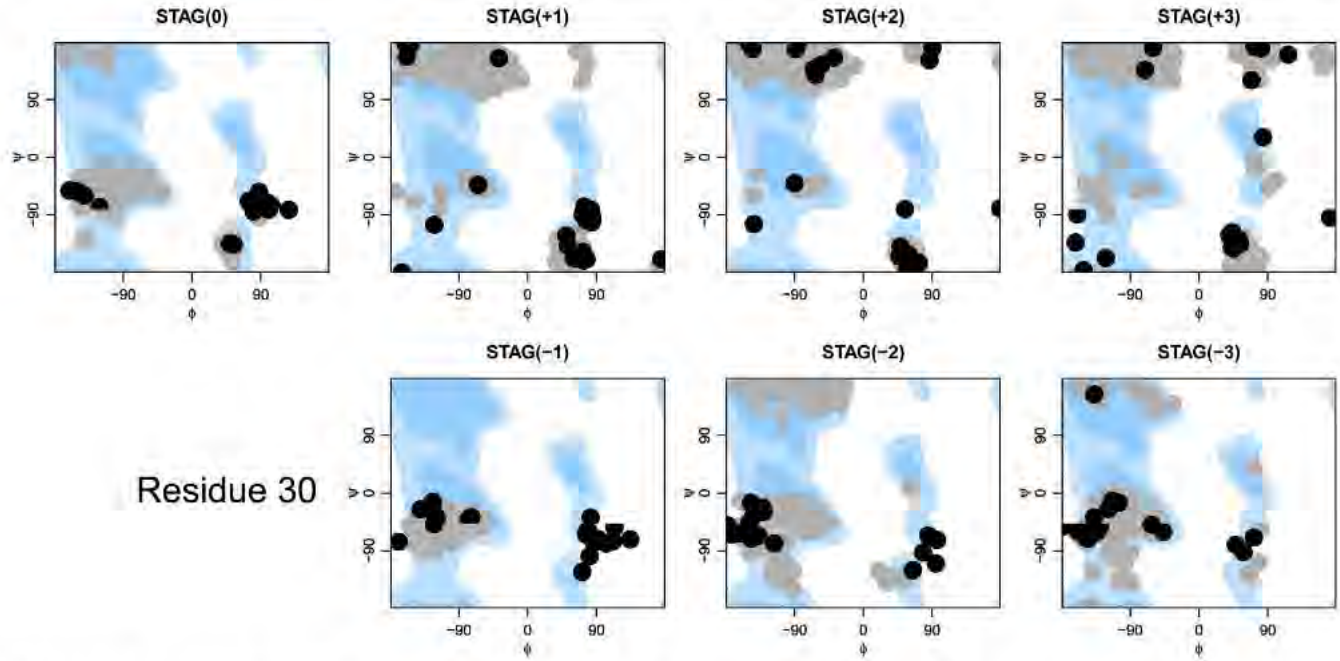

Fig. 3. Ramachandran plot of residue 30 of the 20 central chains at the beginning (20 closed black circles) and at the end of each of the 10 runs (20 chains × 10 runs, closed gray circles). Blue contours in the background show favored regions in the Ramachandran plot of non-proline and non-glycine residues. In positive staggers, the residue's backbone settles primarily in the β sheet region while in zero and negative staggers, the residue settles primarily in the α helical region of the plot.

correlates well with the degree of stagger, especially for the negative staggers.

Stagger 0 does not develop a significant twist in any of the 10 runs. To investigate the effect of simulation length, we extended two of the runs from 10 ns to 90 ns. The red dots in Fig. 2 correspond to the extended simulations (averaged over the last 10 ns of 90 ns). Figs. S3–9 in Supporting materials contains the time evolution of the twist of the extended runs in all staggers. The fibril exhibits torsional fluctuations around the fiber axis with a mean twist of 0°.

Staggers +1 and 1 show slight preference for right and left handed turns, respectively, whereas a few runs of both staggers develop little/no twist after 10 ns. But when 2 of the 10 runs were extended to 90 ns, the twist in both staggers reverts to 0 and the fibrils oscillate around the *z* axis.

During the 10 ns simulations, staggers +2 and 2, diverge significantly. All runs of stagger +2 develop right handed twist of relatively smaller magnitude compared to stagger 2 which develops left handed turns of ~4° per chain. When 2 of the 10 runs in either stagger are extended to 90 ns, stagger +2 reverts back to the starting twist of 0 or a slight positive twist while stagger 2 stabilizes at 8.44° ± 0.28 or 5.7° ± 0.4 respectively (see Fig. S8).

During the 10 ns simulations, staggers +3 and 3 diverge further with stagger +3 developing a right handed twist of 2° per chain while stagger 3 develops a left handed twist of ~5° per chain. When extended to 90 ns, one of the two runs with stagger +3 shows a slight positive twist while the other shows a slight negative twist. After 90 ns, neither runs with stagger 3 stabilize. During the last 10 ns, one run has a twist of 4.52° ± 0.38 while the other has a twist of 9.6° ± 0.4.

Taken together, only staggers 2 and 3 show a twist of significant magnitude and they are both left-handed. By the end of 90 ns, stagger 2 reaches a stable state while stagger 3 does not. In stagger 3 the loop is stretched – possibly rendering the structure unstable. Thus stagger 2 emerges as a possible candidate for the physiologically relevant structure.

The inter chain distance in all the simulations increases from an initial value of 4.8 Åto 4.9 ± 0.3 Å. The values remain in this range in all the simulations (both 10 ns and 90 ns). Further, the development of twist seems to be a property of the U-shaped fibril since studies (not shown) of only 20 chains along the *z*-axis – without the benefit of $M35_{top}$–$M35_{bottom}$ hydrophobic patch – also show comparable twist.

Since only negative staggers generate left-handed helices and the magnitude of twist also correlates well with the stagger, it is possible that negative staggers are the biologically relevant conformations. Another amyloid-like fibril forming peptide, the 37 amino acid long amylin peptide, has recently been found to also develop left-handed twist [85]. Further, the amyloid fibers formed by the N-terminal sequence of serum amyloid A (SAA-12) are always right-handed [71]. These findings support the argument that the twisting properties of aggregates are encoded in the sequence of the aggregating peptide. It has long been known that β sheets formed by a contiguous protein chain mostly have a right-handed twist [86]. It has also been proposed that steric hindrance between the side chain C_β and backbone carbonyl oxygen explains the right-handed twist in antiparallel β sheets [87]. However, in the case of amyloid-type aggregation, the β sheets are formed between different chains. We calculated the difference between the pair interaction energy of C_β–$O_{backbone}$ at the start and end of a 10 ns run of each stagger and the averaged values are shown in Fig. S10. Pair energy decreases in all staggers – twisted or untwisted. Stagger 3 shows the maximum decrease in energy followed closely by 2 and 0. The analysis suggests that in amyloid β sheets, both right and left handed twists can help relieve the C_β–$O_{backbone}$ steric clash. However, the approximate nature of energy analysis used here together with the observation that there is little difference between the stagger 2 and 0 suggests that a more detailed analysis would be required to pinpoint the molecular mechanism underlying the observed relationship.

3.2. Role of Salt-bridges

In the current study, the magnitude of the stagger is limited by the length of the loop. Large staggers lead to a stretched loop in the hairpin structure. K28 is part of the loop and forms a salt bridge

with D23 which has been found to be critical for hairpin formation and stability. Depending on the sign and magnitude of stagger that dictates the length of the loop, D23 of chain i can form salt bridges with K28 of chain i, $i \pm 1$, $i \pm 2$ or $i \pm 3$. To study the interplay between stagger and salt bridges, salt bridges involving residues D23 and K28 were investigated. A salt bridge was considered to exist if a D23 residue was within a distance of 3.2 Åfrom a K28 residue. In stagger 0, $D23_i$ can form a salt bridge with $K28_i$, $K28_{i+1}$ or $K28_{i\ \ 1}$, sometimes with all three (subscripts indicate chain numbers). Table 2 has details of all staggers. Fig. S11–14 in the supporting material contain results of one (of ten) run from each stagger. It is both interesting and intuitive to see different salt bridge pairs at different staggers.

3.3. Ramachandran plots of the peptide backbone

When the structure of one stagger is compared to that of another, notable differences are observed in the backbone dihedral angles in the residue range 25–30 only (GSNKGA). Ramachandran plot of residue 30 shown in Fig. 3 reveals that the backbone dihedral angles of the 20 chains at the beginning (20 filled black circles) of the simulation gravitate from unfavorable regions to more favorable regions. Contour plots in the background show favored (dark blue) and generously allowed (light blue) regions in the Ramachandran plot [88]. A clear distinction between positive and negative staggers emerges from this plot. Residue 30 in the positive staggers settles primarily in the β sheet region of Ramachandran plot while the same residue in negative staggers settles in α helical region of the plot. Zero stagger also settles in the α helical region of the plot. Ramachandran plots of residues 25–29 of 20 central chains (10 each on the top and bottom) at the beginning and at the end of the 10 ns runs are shown in the supporting material (Figs. S15–20). Residues 25 and 29 are both glycines and the lack of a side chain imparts higher flexibility and allows them to explore larger area in the Ramachandran plot compared to other residues [88,89]. K28 in staggers 0, ±1, and ±2 all occupy allowed regions in the Ramachandran plot while staggers ±3 explore disallowed/generously-allowed regions in $\phi > 90$. Definite conclusions cannot be drawn from residues 27 and 29 since they flank residue K28 that forms a salt bridge with D23. The formation of this salt bridge indirectly affects the backbone torsions of residues 27 and 29. Collectively the plots reveal that staggers of large magnitude can lead the backbone torsions of the loop residues to explore greater conformational space and even venture into disallowed regions at some point during the simulations, although this is not generally true of stagger 2. This together with the direction and magnitude of fibril twist in the extended simulations strongly supports stagger 2 as a candidate for the physiologically relevant β hairpin structure. The salt bridge pairs along with backbone dihedrals in the loop region offer insights into the directional preference of the staggers. Determining the exact residue(s) responsible for the twisting behavior will require careful single-site or mutiple-site mutagenesis experiments. These efforts are beyond the scope of the current work.

4. Conclusions

The helical amyloid β-sheets are always left handed but there exists no consensus on the exact stagger of the sheets. We demonstrated in this study that twist of the fibrils is strongly affected by the initial stagger. Our study suggests that negative staggers (specifically stagger 2) could be the physiologically relevant structure that leads to the experimentally observed left-handed helix. This underscores the importance of conducting further experimental studies to determine the exact stagger–twist relationship of the fibrils. But given the inherent polymorphism observed in amyloid secondary structures, it is entirely possible that a variety of staggers and a range of values of helical twist occur in nature. This possibility complicates the task of development of drugs that need to be designed for a variety of Aβ structures. The current work also shows how atomistic simulations can build on experimental efforts to help clarify the details of macromolecular structure.

Acknowledgments

This research was sponsored by the US Department of Energy (DOE) under Contract No. DE-AC05-00OR22725 with UT-Battelle, LLC managing contractor for Oak Ridge National Laboratory. This research used resources of the National Energy Research Scientific Computing Center, which is supported by the Office of Science of the US Department of Energy under Contract No. DE-AC02-05CH11231. P.K.G. thanks Dr. Robert Tycko and Dr. Cyril Falvo for useful discussions. We thank the anonymous reviewers for insightful comments that greatly improved the manuscript.

Appendix A. Supplementary data

Supplementary data associated with this article can be found, in the online version, at http://dx.doi.org/10.1016/j.febslet.2013.06.050.

References

[1] Chiti, F. and Dobson, C.M. (2006) Protein misfolding, functional amyloid, and human disease. Ann. Rev. Biochem. 75 (1), 333–366.
[2] Bucciantini, M., Giannoni, E., Chiti, F., Baroni, F., Formigli, L., Zurdo, J., Taddei, N., Ramponi, G., Dobson, C.M. and Stefani, M. (2002) Inherent toxicity of aggregates implies a common mechanism for protein misfolding diseases. Nature 416, 507–511.
[3] Alzheimer's Association, Thies, W. and Bleiler, L. (2011) Alzheimer's disease facts and figures. Alzheimers Dement. 7, 208–244.
[4] Goate, A., Chartier-Harlin, M.C., Mullan, M., Brown, J., Crawford, F., Fidani, L., Giuffra, L., Haynes, A., Irving, N. and James, L. (1991) Segregation of a missense mutation in the amyloid precursor protein gene with familial Alzheimer's disease. Nature 349, 704–706.
[5] Iwatsubo, T., Odaka, A., Suzuki, N., Mizusawa, H., Nukina, N. and Ihara, Y. (1994) Visualization of A β 42(43) and A β 40 in senile plaques with end-specific A β monoclonals: evidence that an initially deposited species is A β 42(43). Neuron 13, 45–53.
[6] Iwatsubo, T., Mann, D.M., Odaka, A., Suzuki, N. and Ihara, Y. (1995) Amyloidβ protein (Aβ) deposition: Aβ42(43) precedes Aβ40 in Down syndrome. Ann. Neurol. 37, 294–299.
[7] Petkova, A.T., Yau, W.-M. and Tycko, R. (2005) Experimental constraints on quaternary structure in Alzheimer's β-amyloid fibrils. Biochemistry 45, 498–512.
[8] Lührs, T., Ritter, C., Adrian, M., Riek-Loher, D., Bohrmann, B., Döbeli, H., Schubert, D. and Riek, R. (2005) 3D structure of Alzheimer's amyloid-β(1–42) fibrils. Proc. Natl. Acad. Sci. 102, 17342–17347.
[9] Fändrich, M., Schmidt, M. and Grigorieff, N. (2011) Recent progress in understanding Alzheimer's β-amyloid structures. Trends Biochem. Sci. 36, 338–345.
[10] Hilbich, C., Kisters-Woike, B., Reed, J., Masters, C.L. and Beyreuther, K. (1991) Aggregation and secondary structure of synthetic amyloid β A4 peptides of Alzheimer's disease. J. Mol. Biol. 218, 149–163.
[11] Sunde, M. and Blake, C.C. (1998) From the globular to the fibrous state: protein structure and structural conversion in amyloid formation. Q. Rev. Biophys. 31, 1–39.
[12] Serpell, L.C. and Smith, J.M. (2000) Direct visualisation of the β-sheet structure of synthetic Alzheimer's amyloid. J. Mol. Biol. 299, 225–231.
[13] Oyler, N.A. and Tycko, R. (2004) Absolute structural constraints on amyloid fibrils from solid-state NMR spectroscopy of partially oriented samples. J. Am. Chem. Soc. 126, 4478–4479.
[14] Antzutkin, O.N., Balbach, J.J., Leapman, R.D., Rizzo, N.W., Reed, J. and Tycko, R. (2000) Multiple quantum solid-state NMR indicates a parallel, not antiparallel, organization of β-sheets in Alzheimer's β-amyloid fibrils. Proc. Natl. Acad. Sci. 97, 13045–13050.
[15] Balbach, J.J., Ishii, Y., Antzutkin, O.N., Leapman, R.D., Rizzo, N.W., Dyda, F., Reed, J. and Tycko, R. (2000) Amyloid fibril formation by Aβ16–22, a seven-residue fragment of the Alzheimer's β-amyloid peptide, and structural characterization by Solid State NMR. Biochemistry 39, 13748–13759.
[16] Antzutkin, O.N., Balbach, J.J. and Tycko, R. (2003) Site-specific identification of non-β-strand conformations in Alzheimer's β-amyloid fibrils by solid-state NMR. Biophys. J. 84, 3326–3335.

[17] Petkova, A.T., Ishii, Y., Balbach, J.J., Antzutkin, O.N., Leapman, R.D., Delaglio, F. and Tycko, R. (2002) A structural model for Alzheimer's β-amyloid fibrils based on experimental constraints from solid state NMR. Proc. Natl. Acad. Sci. 99, 16742–16747.
[18] Petkova, A.T., Leapman, R.D., Guo, Z., Yau, W.-M., Mattson, M.P. and Tycko, R. (2005) Self-propagating, molecular-level polymorphism in Alzheimer's β-amyloid fibri ls. Science 307, 262–265.
[19] Jaroniec, C.P., MacPhee, C.E., Astrof, N.S., Dobson, C.M. and Griffin, R.G. (2002) Molecular conformation of a peptide fragment of transthyretin in an amyloid fibril. Proc. Natl. Acad. Sci. 99, 16748–16753.
[20] Jaroniec, C.P., MacPhee, C.E., Bajaj, V.S., McMahon, M.T., Dobson, C.M. and Griffin, R.G. (2004) High-resolution molecular structure of a peptide in an amyloid fibril determined by magic angle spinning NMR spectroscopy. Proc. Natl. Acad. Sci. 101, 711–716.
[21] Ritter, C., Maddelein, M.-L., Siemer, A.B., Luhrs, T., Ernst, M., Meier, B.H., Saupe, S.J. and Riek, R. (2005) Correlation of structural elements and infectivity of the HET-s prion. Nature 435, 844–848.
[22] Benzinger, T.L.S., Gregory, D.M., Burkoth, T.S., Miller-Auer, H., Lynn, D.G., Botto, R.E. and Meredith, S.C. (2000) Two-dimensional structure of β-amyloid(10–35) fibrils. Biochemistry 39, 3491–3499.
[23] Gregory, D.M., Benzinger, T.L., Burkoth, T.S., Miller-Auer, H., Lynn, D.G., Meredith, S.C. and Botto, R.E. (1998) Dipolar recoupling NMR of biomolecular self-assemblies: determining inter- and intrastrand distances in fibrilized Alzheimer's β-amyloid peptide. Solid State Nucl. Magn. Reson. 13, 149–166.
[24] Heller, J., Kolbert, A.C., Larsen, R., Ernst, M., Bekker, T., Baldwin, M., Prusiner, S.B., Pines, A. and Wemmer, D.E. (1996) Solid-state NMR studies of the prion protein H1 fragment. Protein Sci. 5, 1655–1661.
[25] Laws, D.D., Bitter, H.-M.L., Liu, K., Ball, H.L., Kaneko, K., Wille, H., Cohen, F.E., Prusiner, S.B., Pines, A. and Wemmer, D.E. (2001) Solid-state NMR studies of the secondary structure of a mutant prion protein fragment of 55 residues that induces neurodegeneration. Proc. Natl. Acad. Sci. 98, 11686–11690.
[26] Naito, A., Kamihira, M., Inoue, R. and Saitō, H. (2004) Structural diversity of amyloid fibril formed in human calcitonin as revealed by site-directed ^{13}C solid-state NMR spectroscopy. Magn. Reson. Chem 42, 247–257.
[27] Halverson, K.J., Sucholeiki, I., Ashburn, T.T. and Lansbury, P.T. (1991) Location of β-sheet-forming sequences in amyloid proteins by FTIR. J. Am. Chem. Soc. 113, 6701–6703.
[28] Zandomeneghi, G., Krebs, M.R.H., McCammon, M.G. and Fändrich, M. (2004) FTIR reveals structural differences between native β-sheet proteins and amyloid fibrils. Protein Sci. 13, 3314–3321.
[29] Khurana, R. and Fink, A.L. (2000) Do parallel β-helix proteins have a unique fourier transform infrared spectrum? Biophys. J. 78, 994–1000.
[30] Serpell, L.C. (2000) Alzheimer's amyloid fibrils: structure and assembly. Biochim. Biophys. Acta 1502, 16–30.
[31] Sunde, M., Serpell, L.C., Bartlam, M., Fraser, P.E., Pepys, M.B. and Blake, C.C. (1997) Common core structure of amyloid fibrils by synchrotron X-ray diffraction. J. Mol. Biol. 273, 729–739.
[32] Fraser, P.E., Nguyen, J.T., Inouye, H., Surewicz, W.K., Selkoe, D.J., Podlisny, M.B. and Kirschner, D.A. (1992) Fibril formation by primate, rodent, and Dutch-hemorrhagic analogues of Alzheimer amyloid β-protein. Biochemistry 31, 10716–10723.
[33] Eanes, E.D. and Glenner, G.G. (1968) X-ray diffraction studies on amyloid filaments. J. Histochem. Cytochem. 16, 673–677.
[34] Kheterpal, I., Zhou, S., Cook, K.D. and Wetzel, R. (2000) Aβ amyloid fibrils possess a core structure highly resistant to hydrogen exchange. Proc. Natl. Acad. Sci. 97, 13597–13601.
[35] Hoshino, M., Katou, H., Hagihara, Y., Hasegawa, K., Naiki, H. and Goto, Y. (2002) Mapping the core of the β2-microglobulin amyloid fibril by H/D exchange. Nat. Struct. Mol. Biol. 9, 332–336.
[36] Ippel, J.H., Olofsson, A., Schleucher, J., Lundgren, E. and Wijmenga, S.S. (2002) Probing solvent accessibility of amyloid fibrils by solution NMR spectroscopy. Proc. Natl. Acad. Sci. 99, 8648–8653.
[37] Kuwata, K., Matumoto, T., Cheng, H., Nagayama, K., James, T.L. and Roder, H. (2003) NMR-detected hydrogen exchange and molecular dynamics simulations provide structural insight into fibril formation of prion protein fragment 106–126. Proc. Natl. Acad. Sci. 100, 14790–14795.
[38] Yamaguchi, K.-i., Katou, H., Hoshino, M., Hasegawa, K., Naiki, H. and Goto, Y. (2004) Core and heterogeneity of β2-microglobulin amyloid fibrils as revealed by H/D exchange. J. Mol. Biol. 338, 559–571.
[39] Olofsson, A., Ippel, J.H., Wijmenga, S.S., Lundgren, E. and Öhman, A. (2004) Probing solvent accessibility of transthyretin amyloid by solution NMR spectroscopy. J. Biol. Chem. 279, 5699–5707.
[40] Wang, S.S.S., Tobler, S.A., Good, T.A. and Fernandez, E.J. (2003) Hydrogen exchange-mass spectrometry analysis of β-amyloid peptide structure. Biochemistry 42, 9507–9514.
[41] Whittemore, N.A., Mishra, R., Kheterpal, I., Williams, A.D., Wetzel, R. and Serpersu, E.H. (2005) Hydrogen–deuterium (H/D) exchange mapping of Aβ1–40 amyloid fibril secondary structure using nuclear magnetic resonance spectroscopy. Biochemistry 44, 4434–4441.
[42] Thakur, A.K. and Wetzel, R. (2002) Mutational analysis of the structural organization of polyglutamine aggregates. Proc. Natl. Acad. Sci. 99, 17014–17019.
[43] Williams, A.D., Portelius, E., Kheterpal, I., Guo, J.-t. T., Cook, K.D., Xu, Y. and Wetzel, R. (2004) Mapping aβ amyloid fibril secondary structure using scanning proline mutagenesis. J. Mol. Biol. 335, 833–842.
[44] Jayasinghe, S.A. and Langen, R. (2004) Identifying structural features of fibrillar islet amyloid polypeptide using site-directed spin labeling. J. Biol. Chem. 279, 48420–48425.
[45] Der-Sarkissian, A., Jao, C.C., Chen, J. and Langen, R. (2003) Structural organization of α-synuclein fibrils studied by site-directed spin labeling. J. Biol. Chem. 278, 37530–37535.
[46] Török, M., Milton, S., Kayed, R., Wu, P., McIntire, T., Glabe, C.G. and Langen, R. (2002) Structural and dynamic features of Alzheimer's Aβ peptide in amyloid fibrils studied by site-directed spin labeling. J. Biol. Chem. 277, 40810–40815.
[47] Dong, J., Atwood, C.S., Anderson, V.E., Siedlak, S.L., Smith, M.A., Perry, G. and Carey, P.R. (2003) Metal binding and oxidation of amyloid-β within isolated senile plaque cores: Raman microscopic evidence. Biochemistry 42, 2768–2773.
[48] Fawzi, N.L.L., Kohlstedt, K.L., Okabe, Y. and Head-Gordon, T. (2008) Protofibril assemblies of the arctic, Dutch, and Flemish mutants of the Alzheimer's Aβ1–40 peptide. Biophys. J. 94, 2007–2016.
[49] Urbanc, B., Cruz, L., Ding, F., Sammond, D., Khare, S., Buldyrev, S.V., Stanley, H.E. and Dokholyan, N.V. (2004) Molecular dynamics simulation of amyloid β dimer formation. Biophys. J. 87, 2310–2321.
[50] Jahn, T.R., Makin, O.S., Morris, K.L., Marshall, K.E., Tian, P., Sikorski, P. and Serpell, L.C. (2010) The common architecture of cross-β amyloid. J. Mol. Biol. 395, 717–727.
[51] Paravastu, A.K., Leapman, R.D., Yau, W.-M. and Tycko, R. (2008) Molecular structural basis for polymorphism in Alzheimer's β-amyloid fibrils. Proc. Natl. Acad. Sci. 105, 18349–18354.
[52] Miller, Y., Ma, B. and Nussinov, R. (2011) The unique Alzheimer's β-amyloid triangular fibril has a cavity along the fibril axis under physiological conditions. J. Am. Chem. Soc. 133, 2742–2748.
[53] Ma, B. and Nussinov, R. (2002) Stabilities and conformations of Alzheimer's β-amyloid peptide oligomers (Aβ16–22, Aβ16–35, and Aβ10–35): sequence effects. Proc. Natl. Acad. Sci. 99, 14126–14131.
[54] Zanuy, D. and Nussinov, R. (2003) The sequence dependence of fiber organization. A comparative molecular dynamics study of the islet amyloid polypeptide segments 22–27 and 22–29. J. Mol. Biol. 329, 565–584.
[55] Ma, B. and Nussinov, R. (2006) The stability of monomeric intermediates controls amyloid formation: Aβ25–35 and its N27Q mutant. Biophys. J. 90, 3365–3374.
[56] Wei, G., Jewett, A.I. and Shea, J.-E.E. (2010) Structural diversity of dimers of the Alzheimer amyloid-β(25–35) peptide and polymorphism of the resulting fibrils. Phys. Chem. Chem. Phys. 12, 3622–3629.
[57] Miller, Y., Ma, B. and Nussinov, R. (2010) Polymorphism in Alzheimer Aβ amyloid organization reflects conformational selection in a rugged energy landscape. Chem. Rev. 110, 4820–4838.
[58] Buchete, N.-V.V. and Hummer, G. (2007) Structure and dynamics of parallel β-sheets, hydrophobic core, and loops in Alzheimer's A β fibrils. Biophys. J. 92, 3032–3039.
[59] Buchete, N.-V.V., Tycko, R. and Hummer, G. (2005) Molecular dynamics simulations of Alzheimer's β-amyloid protofilaments. J. Mol. Biol. 353, 804–821.
[60] Baumketner, A. and Shea, J.-E.E. (2007) The structure of the Alzheimer amyloid β 10–35 peptide probed through replica-exchange molecular dynamics simulations in explicit solvent. J. Mol. Biol. 366, 275–285.
[61] Gorevic, P.D., Castano, E.M., Sarma, R. and Frangione, B. (1987) Ten to fourteen residue peptides of Alzheimer's disease protein are sufficient for amyloid fibril formation and its characteristic X-ray diffraction pattern. Biochem. Biophys. Res. Commun. 147 (3), 854–862.
[62] Kirschner, D.A., Inouye, H., Duffy, L.K., Sinclair, A., Lind, M. and Selkoe, D.J. (1987) Synthetic peptide homologous to β protein from Alzheimer disease forms amyloid-like fibrils in vitro. Proc. Natl. Acad. Sci. 84, 6953–6957.
[63] Fraser, P.E., McLachlan, D.R., Surewicz, W.K., Mizzen, C.A., Snow, A.D., Nguyen, J.T. and Kirschner, D.A. (1994) Conformation and fibrillogenesis of Alzheimer A β peptides with selected substitution of charged residues. J. Mol. Biol. 244, 64–73.
[64] Sikorski, P., Atkins, E.D. and Serpell, L.C. (2003) Structure and texture of fibrous crystals formed by Alzheimer's aβ(11–25) peptide fragment. Structure (London, England : 1993) 11, 915–926.
[65] Liang, Y., Pingali, S.V.V., Jogalekar, A.S., Snyder, J.P., Thiyagarajan, P. and Lynn, D.G. (2008) Cross-strand pairing and amyloid assembly. Biochemistry 47, 10018–10026.
[66] Chen, Z., Krause, G. and Reif, B. (2005) Structure and orientation of peptide inhibitors bound to β-amyloid fibrils. J. Mol. Biol. 354, 760–776.
[67] Bu, Z., Shi, Y., Callaway, D.J. and Tycko, R. (2007) Molecular alignment within β-sheets in Aβ(14–23) fibrils: solid-state NMR experiments and theoretical predictions. Biophys. J. 92, 594–602.
[68] Hughes, E., Burke, R.M. and Doig, A.J. (2000) Inhibition of toxicity in the β-amyloid peptide fragment β-(25–35) using N-methylated derivatives: a general strategy to prevent amyloid formation. J. Biol. Chem. 275, 25109–25115.
[69] Sawaya, M.R., Sambashivan, S., Nelson, R., Ivanova, M.I., Sievers, S.A., Apostol, M.I., Thompson, M.J., Balbirnie, M., Wiltzius, J.J.W., McFarlane, H.T., Madsen, A.O., Riekel, C. and Eisenberg, D. (2007) Atomic structures of amyloid cross-beta; spines reveal varied steric zippers. Nature 447, 453–457.

Please cite this article in press as: GhattyVenkataKrishna, P.K., et al. Effect of the amyloid β hairpin's structure on the handedness of helices formed by its aggregates. FEBS Lett. (2013), http://dx.doi.org/10.1016/j.febslet.2013.06.050

[70] Xu, W., Zhang, C., Derreumaux, P., Gräslund, A., Morozova-Roche, L. and Mu, Y. (2011) Intrinsic Determinants of Aβ12–24 pH-dependent self-assembly revealed by combined computational and experimental studies. PLoS One 6, e24329.
[71] Rubin, N., Perugia, E., Goldschmidt, M., Fridkin, M. and Addadi, L. (2008) Chirality of amyloid suprastructures. J. Am. Chem. Soc. 130, 4602–4603.
[72] Selkoe, D.J. (2001) Alzheimer's disease: genes, proteins, and therapy. Physiol. Rev. 81, 741–766.
[73] Wei, W., Norton, D.D., Wang, X. and Kusiak, J.W. (2002) Aβ 17–42 in Alzheimer's disease activates JNK and caspase-8 leading to neuronal apoptosis. Brain 125, 2036–2043.
[74] Lalowski, M., Golabek, A., Lemere, C.A., Selkoe, D.J., Wisniewski, H.M., Beavis, R.C., Frangione, B. and Wisniewski, T. (1996) The "nonamyloidogenic" p3 fragment (amyloid β17–42) is a major constituent of Down's syndrome cerebellar preamyloid. J. Biol. Chem. 271, 33623–33631.
[75] Fawzi, N.L., Okabe, Y., Yap, E.-H. and Head-Gordon, T. (2007) Determining the critical nucleus and mechanism of fibril elongation of the Alzheimer's Aβ(1–40) peptide. J. Mol. Biol. 365, 535–550.
[76] Zheng, J., Jang, H., Ma, B., Tsai, C.-J. and Nussinov, R. (2007) Modeling the Alzheimer Aβ17–42 fibril architecture: tight intermolecular sheet-sheet association and intramolecular hydrated cavities. Biophys. J. 93 (9), 3046–3057.
[77] Makin, O.S. and Serpell, L.C. (2005) Structures for amyloid fibrils. FEBS J. 272, 5950–5961.
[78] Blake, C. and Serpell, L. (1996) Synchrotron X-ray studies suggest that the core of the transthyretin amyloid fibril is a continuous beta-sheet helix. Structure (London, England : 1993) 4, 989–998.
[79] Phillips, J.C., Braun, R., Wang, W., Gumbart, J., Tajkhorshid, E., Villa, E., Chipot, C., Skeel, R.D., Kalé, L. and Schulten, K. (2005) Scalable molecular dynamics with NAMD. J. Comput. Chem. 26, 1781–1802.
[80] MacKerell, A.D., Bashford, D., Bellott, Dunbrack, R.L., Evanseck, J.D., Field, M.J., Fischer, S., Gao, J., Guo, H., Ha, S., Joseph-McCarthy, D., Kuchnir, L., Kuczera, K., Lau, F.T.K., Mattos, C., Michnick, S., Ngo, T., Nguyen, D.T., Prodhom, B., Reiher, W.E., Roux, B., Schlenkrich, M., Smith, J.C., Stote, R., Straub, J., Watanabe, M., Wiórkiewicz-Kuczera, J., Yin, D. and Karplus, M. (1998) All-atom empirical potential for molecular modeling and dynamics studies of proteins. J. Phys. Chem. B 102, 3586–3616.
[81] Mackerell, A.D., Feig, M. and Brooks, C.L. (2004) Extending the treatment of backbone energetics in protein force fields: limitations of gas-phase quantum mechanics in reproducing protein conformational distributions in molecular dynamics simulations. J. Comput. Chem. 25, 1400–1415.
[82] Martyna, G.J., Tobias, D.J. and Klein, M.L. (1994) Constant pressure molecular dynamics algorithms. J. Chem. Phys. 101 (5), 4177–4189.
[83] Feller, S.E., Zhang, Y., Pastor, R.W. and Brooks, B.R. (1995) Constant pressure molecular dynamics simulation: the Langevin piston method. J. Chem. Phys. 103 (11), 4613–4621.
[84] Humphrey, W., Dalke, A. and Schulten, K. (1996) VMD: visual molecular dynamics. J. Mol. Graph. 14, 33–38.
[85] Xu, W., Su, H., Zhang, J.Z.H. and Mu, Y. (2012) Molecular dynamics simulation study on the molecular structures of the amylin fibril models. J. Phys. Chem. B 116, 13991–13999.
[86] Chothia, C. (1973) Conformation of twisted beta-pleated sheets in proteins. J. Mol. Biol. 75, 295–302.
[87] Yang, A.S. and Honig, B. (1995) Free energy determinants of secondary structure formation: II. Antiparallel β-sheets. J. Mol. Biol. 252, 366–376.
[88] Lovell, S.C., Davis, I.W., Arendall, W.B., de Bakker, P.I.W., Word, J.M., Prisant, M.G., Richardson, J.S. and Richardson, D.C. (2003) Structure validation by Cα geometry: ϕ, ψ and Cβ deviation. Proteins 50, 437–450.
[89] Ho, B. and Brasseur, R. (2005) The Ramachandran plots of glycine and pre-proline. BMC Struct. Biol. 5 (1), 14.

Please cite this article in press as: GhattyVenkataKrishna, P.K., et al. Effect of the amyloid β hairpin's structure on the handedness of helices formed by its aggregates. FEBS Lett. (2013), http://dx.doi.org/10.1016/j.febslet.2013.06.050